J Mater Sci (2008) 43:6724–6733
DOI 10.1007/s10853-008-2620-3

Analysis of the structure and deformation of a woven composite lamina using X-ray microdiffraction

Richard J. Davies · Stephen J. Eichhorn · James A. Bennett · Christian Riekel · Robert J. Young

Received: 21 March 2008 / Accepted: 26 March 2008 / Published online: 31 July 2008

Abstract X-ray diffraction (XRD) is an important tool for studying multiphase materials because it can resolve parameters from each phase independently. When coupled with a high-flux, microfocussed X-ray beam, scanning microdiffraction experiments are possible. This technique can investigate how reciprocal-space parameters vary as a function of real-space sample geometry for heterogeneous materials. Consequently, multiphase materials can be imaged in terms of those parameter variations. This study reports on the use of microfocussed X-ray diffraction (μXRD) to both image and follow the deformation of a multiphase material. In this case, this technique is applied to the study of a woven fibre-reinforced composite (FRC) lamina. Such systems are difficult to study with other experimental techniques because the fibres are inaccessible and the matrix is often opaque. However, using μXRD it is possible to assess both sample geometry and stress field information simultaneously.

Introduction

X-ray diffraction (XRD) is a powerful tool for studying multiphase materials. This is because a diffraction pattern contains information that is specific to each phase within the illuminated gauge volume. This can include both geometric and structural parameters, many of which are inaccessible to other techniques. Furthermore, this information is collected non-invasively, providing in situ possibilities. Whilst these capabilities already make XRD a powerful technique, it can be considerably enhanced by collecting data in a scanning acquisition mode. This approach allows variations in reciprocal space to be studied as a function of real-space position (on the sample). For this, the spatial resolution is dependent upon the size of the X-ray beam used. As beam size increases, the maximum spatial resolution decreases proportionally. Consequently, microscopic heterogeneities can only be resolved using a high-flux, microfocussed X-ray beam. This limits the technique of scanning microfocussed X-ray diffraction (μXRD) to specialist beamlines at synchrotron radiation (SR) facilities [1].

Fibre-reinforced composites (FRCs) are multiphase materials whose popularity for engineering applications continues to grow. They are, however, notoriously difficult systems to study. Not only are the fibres inaccessible to most experimental techniques, but their performance depends upon a large number of different parameters. Recently, μXRD has been demonstrated as a novel method of investigating their micromechanical properties [2–5]. This relies upon its ability to probe both phases within the illuminated gauge volume simultaneously (in this case the resin and the fibre).

The use of μXRD for FRC studies has, until now, been limited to model composite systems containing single embedded fibres. This geometric simplification limits the analysis to interfacial micromechanics. The mechanical properties of typical engineering composites are, however, governed by many additional parameters. These include inter-fibre friction, off-axis loading and inter-yarn/inter-lamina stress transfer. This is because, unlike model

R. J. Davies · C. Riekel
European Synchrotron Radiation Facility, 6 rue Jules Horowitz, BP220, 38043 Grenoble Cedex, France

S. J. Eichhorn · J. A. Bennett · R. J. Young (✉)
Materials Science Centre, School of Materials, University of Manchester, Grosvenor Street, Manchester M1 7HS, UK
e-mail: robert.young@manchester.ac.uk

composites, engineering applications use complex multi-fibre composites. This includes cross-ply and woven lamina geometries (often termed 'textile structural composites'). A single fibre approach is therefore inadequate to fully investigate their mechanical properties.

A recent publication by the authors [6] reported the use of μXRD to image a FRC with a complex woven lamina geometry. This study reports on the further use of μXRD to investigate the progress of in situ deformation of woven FRC materials. Unlike other test methods, this allows individual contributions towards bulk mechanical properties to be isolated. This is demonstrated for so-called open-hole studies on a woven lamina geometry. The applicability of the technique is demonstrated, highlighting the range of information that can be obtained. This approach particularly emphasises how real- and reciprocal-space information can be combined for novel sample imaging. The study also demonstrates that the μXRD method provides access to information that is inaccessible via other approaches. Furthermore, its current application to model systems [2–5] does not fully exploit the range of information it can provide.

Experimental

Materials

The composite specimen was based upon a satin weave fabric of poly(*p*-phenylene phthalamide) (PPTA) fibre tows impregnated with an epoxy resin matrix and cured at 160 °C. A strip of 200 × 20 mm^2 was cut from the 1.5-mm thick matt aligned with the weave orientation and a resistance strain gauge secured to the specimen using cyanoacrylate adhesive. These samples are compatible with a miniature materials tensile testing rig, and were oriented such that one yarn was always aligned parallel to the deformation axis. For clarity, yarns along this axis will be referred to herein as longitudinal, whilst yarns perpendicular to the deformation axis will be termed transverse. An open-hole geometry was created in the lamina by drilling a ~1 mm diameter hole at the centre of the sample. This design gives a reference position for imaging, allows the stress fields around circular discontinuities to be investigated [7, 8], and replicates the rivet holes used to attach composite panels in aeronautical applications.

A resin impregnated tow of 12 μm PPTA fibres (supplied by Teijin Co. Ltd.) was also investigated without deformation. This specimen had a similar degree of intra- and inter-fibre orientation to the woven sample and allowed the effect of fibre tilt on diffraction patterns to be calibrated.

X-ray microdiffraction

X-ray microdiffraction was carried out at the ID13 beamline of the ESRF [1]. A tensometer (MINIMAT) was installed on the beamline's sample translation stages, with the deformation axis normal to the incoming beam. The beamline was configured with a monochromatic X-ray beam (wavelength = 0.096 nm). For focussing, long focal-length beryllium compound refractive lenses were used. These provide a low-divergence X-ray beam with a spot size at the focal position of 5 μm. An ionisation chamber upstream of the sample position allowed exposure to be normalised to eliminate the influence of storage ring current decay. Typical exposure times were approximately 1 s. All data collection was carried out using a MARCCD 165 detector, rebinned to 1 k × 1 k (a rebinned pixel size of 157.88 μm^2). The beamline setup and experimental geometry used in this study are described elsewhere [6].

During deformation, the force applied to the FRC could be monitored using a calibrated load cell and transducer indicator. A resistance strain gauge attached to each sample also indicated local strain. For each specimen, data sets were then collected at incremental load levels. Each set consisted of a two-dimensional raster-scan, generating a mesh of diffraction patterns over an area surrounding the drilled hole. The scans of the woven sample extended 8 mm around the hole's position. For a scan step size of 200 μm, 1681 diffraction patterns were collected within each woven data set. Figure 1 shows the sample and scan geometry with reference to the deformation axis. An optical image of a similar woven composite is also shown along with a composite image in which individual diffraction patterns are arranged according to their real-space collection position on the sample. From the composite image the position of the hole is clearly visible due to the local reduction in scattering intensity.

Data treatment

Data treatment was carried out using a combination of the Fit2D software application [9] and dedicated batch-processing software designed for treating large data sets [10, 11]. This combination enables automatic data minimisation, analysis and visualisation [10, 11]. In order to calculate meridional reflection intensities, a radial integration was first performed around the detector azimuth. The resulting azimuthal profile consisted of a 360° arc-slice through all 006 layer lines. Each profile was fitted using four Gaussian functions offset by approximately 90°, two being used for each yarn orientation. Spread-estimate fitting algorithms and wrap-around functionality enabled automatic file processing [10]. From the azimuthal position of each Gaussian fit, the in-plane average orientation of the

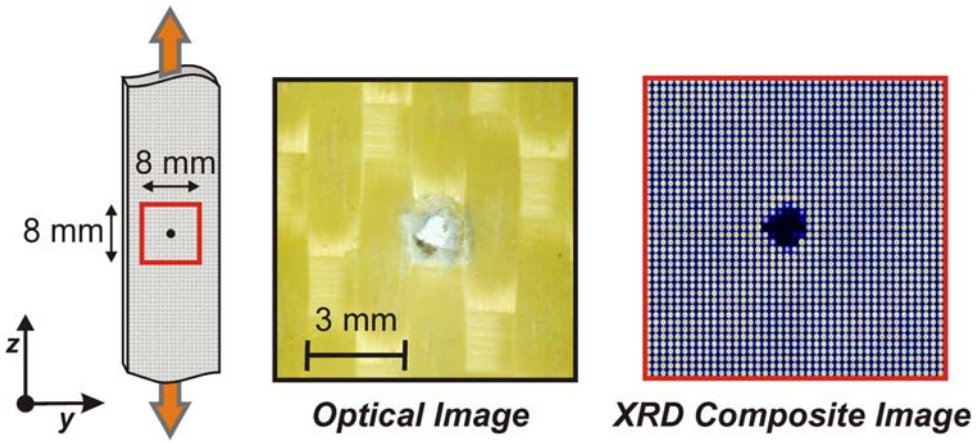

Fig. 1 Schematic of the data collection region with respect to the position of the drilled hole and composite deformation geometry. An optical micrograph of a similar 8×8 mm^2 region of a satin weave composite lamina is also shown along with a composite image comprising individual diffraction patterns placed according to data collection position

fibre axis could be deduced (c^*). This angle was then used to produce radial profiles through the exact centre of each 006 layer line on the diffraction pattern. In this way, a consistent measure of meridional reflection integrated scattering intensity could be determined. A similar approach was used to calculate the radial and azimuthal positions of the meridional and equatorial reflections.

Results and discussion

Figure 2a shows a schematic of transverse and longitudinal yarns within a satin weave FRC sample. The diffraction pattern shown in Fig. 2b corresponds to the pattern that would be obtained from the yellow intersection point. This contains scattering contributions from both the transverse (blue) and longitudinal (red) yarns, where both contributions are superimposed upon one another. It is immediately apparent in Fig. 2b that the individual yarns consist of fibres having a high degree of preferred crystalline domain orientation whilst the yarns themselves exhibit a high degree of inter-fibre alignment. Consequently, the superposition of different yarn orientations within the detector plane can be resolved separately. This is shown in Fig. 2c where the individual contributions arising from the longitudinal and transverse yarns are coloured blue and red, respectively (in accordance with the colour scheme used to represent the two orientations in Fig. 2a). The average in-plane orientation of the two fibre axes are marked c^*.

Each individual diffraction pattern collected in this geometry contains a range of information about the embedded PPTA fibres illuminated within the X-ray beam's 5 μm spot. By plotting different analysis parameters according to their real-space collection position on the sample, their spatial variation can be correlated with the sample's local geometry and stress fields. This information is greatly enhanced by its association with the different yarn orientations within the woven fabric. This makes it possible to build up a much more detailed picture of composite deformation than if information from both yarn orientations were averaged.

Out-of-plane tilt

The effect of out-of-plane fibre axis tilt on the diffraction pattern of a tow of PPTA fibres is illustrated in Fig. 3. The

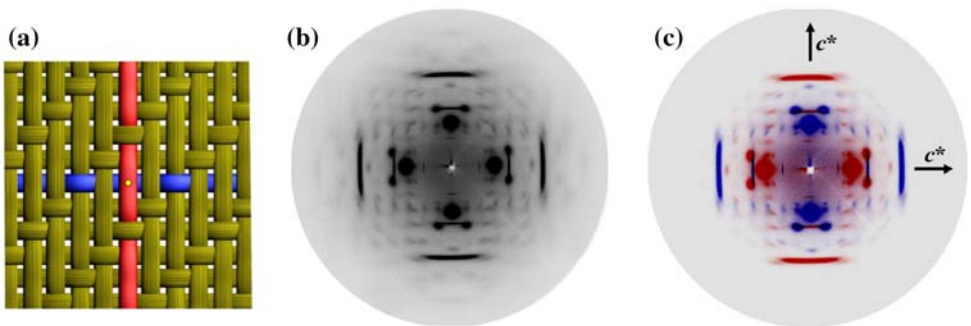

Fig. 2 (**a**) Example of data collection from a position on the sample (indicated by a yellow circle) at which longitudinal (red) and transverse (blue) yarns are superimposed. The resulting diffraction pattern (**b**) shows a superposition of scattering contributions which can be separated by their angular offset (**c**). This allows the two yarn orientations, with their respective fibre axes denoted c^*, to be analysed independently

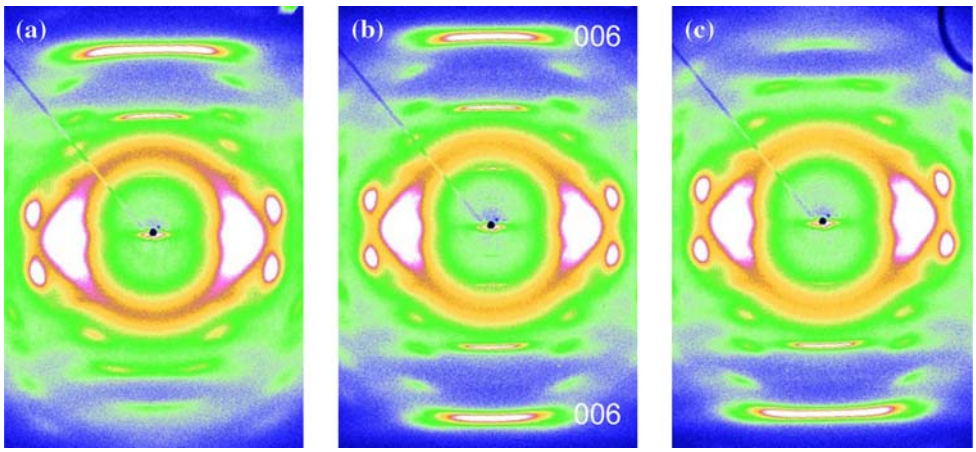

Fig. 3 Diffraction patterns obtained from the PPTA fibre tow tilted at different angles out of the detector plane. (**a**) −15°, (**b**) 0° and (**c**) +15°

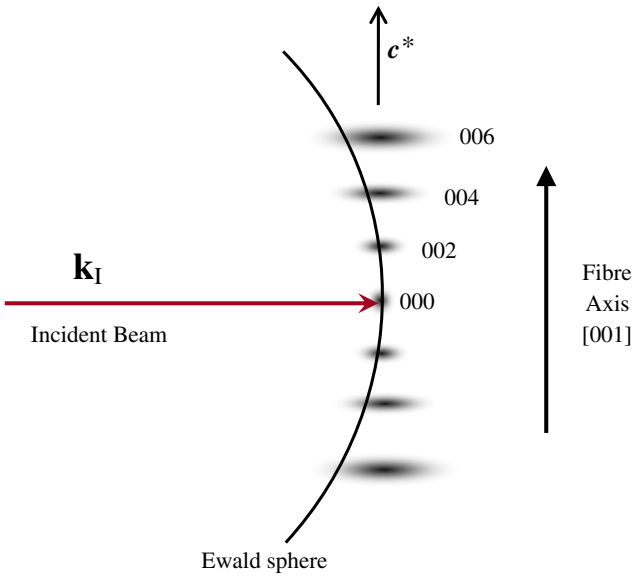

Fig. 4 Schematic diagram illustrating the intersection of the reciprocal lattice along the PPTA [001] fibre axis with the Ewald sphere

relative intensities of the meridional reflections change significantly as the tow is tilted through ± 15°. The reason for this is shown in Fig. 4. With the tow normal to the incoming beam, reciprocal lattice points along [001] (i.e. along the fibre axis) lie on a plane tangential to the surface of the Ewald sphere. Inter- and intra-fibre crystalline domain misorientation gives rise to a distribution around each 00l reciprocal lattice point. This is sufficient to allow an intersection between the reciprocal lattice point distribution and Ewald sphere's surface within each hemisphere. This gives rise to projected reflections on the detector, which in this geometry will be symmetrical and of equal intensity. Tilting the tow out of the detector plane will rotate the 00l distribution mean closer to the Ewald sphere's surface in one hemisphere and further in the other. The resulting variation in relative intensity between meridional reflections can be related to the tilt and angle of the tow [6].

In order to calculate the local tilt angles for the fibres in the woven composite it is necessary to calibrate the effect of the out-of-plane tilt angle upon the relative intensities of the meridional reflections as shown in Fig. 5. The measured intensities of the top and bottom 006 reflections are shown as a function of tilt and in Fig. 5a and it can be seen that they become equal when the tilt angle is ∼0°. By calculating the intensity of the bottom reflection as a fraction of the total intensity, a master calibration curve can be produced, as shown in Fig. 5b. From a function fit to this relationship, average out-of-plane tilt angle can be calculated from the diffraction pattern of any yarn having a similar degree of inter-and intra-fibre orientation.

This capability is demonstrated in Fig. 6 for the average angle of yarn tilt out of the detector plane for both transverse and longitudinal yarns. This parameter has been calculated from each diffraction pattern, and is plotted as an interpolated area plot according to data collection position. Three different strain levels are shown. The results reveal that even relatively complex fabric geometries can be resolved with ease through the resin matrix. The position of the drilled hole is clearly visible at the centre of the scan region (those data points having been reset to zero tilt based upon their lower total scattering intensity). It can be seen that the fabric structure surrounding the hole has not been significantly damaged by the drilling process which can probably be attributed to the constraining effect of the resin. Several studies have previously investigated the effect of drilling on FRC materials [12, 13] and the μXRD technique could provide a new experimental approach for future studies in this field. Figure 6 also shows that the transverse yarns exhibit a lower range of angular tilts compared to longitudinal yarns. This may indicate that the warp yarns are transverse in this specimen (their reduced angular tilt being a consequence of their higher tension during weaving).

Figure 7 shows horizontal and vertical 'slices' taken from the maps of average out-of-plane yarn tilt. The linear

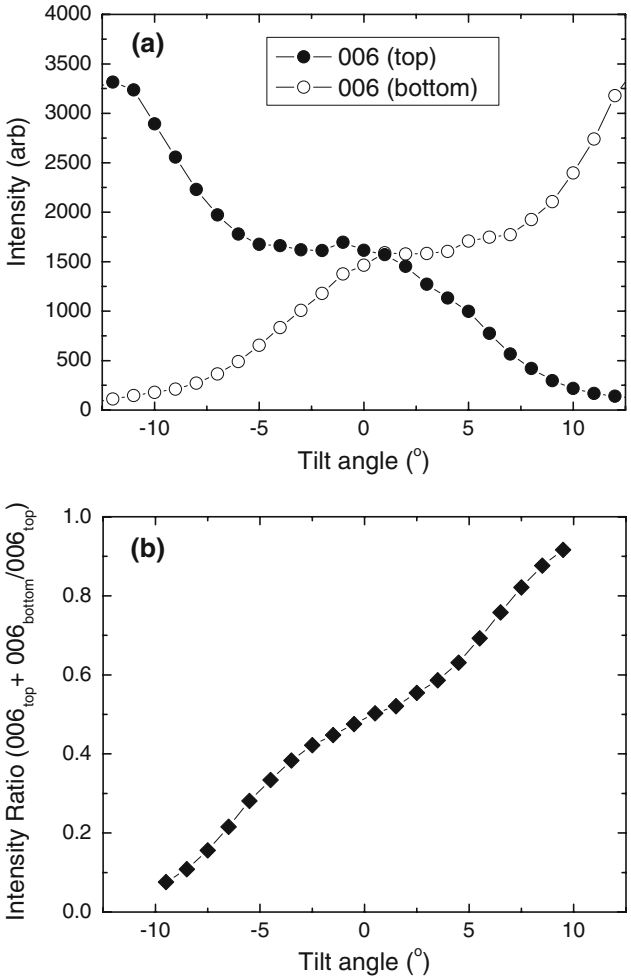

Fig. 5 (**a**) Intensities of the top and bottom 006 reflections in the diffraction pattern of the PPTA fibre tow as a function of angle of tilt out of the detector plane. (**b**) Intensity of top and bottom 006 reflections divided by the intensity of the top reflection as a function of the tilt angle

variation in angle along each slice is shown for the three different strain levels in Fig. 6. In each case, values have been averaged from three consecutive 'rows' or 'columns' taken from the result matrix (to reduce artefacts). Not only can the geometry of the satin weave be easily resolved but a difference is also clearly visible between the tilt of the fibres as a function of applied macroscopic strain. It can be seen that the variation in the angle of tilt of the transverse yarns increases (Fig. 7 top) with strain, whereas it decreases for the longitudinal yarns (Fig. 7 bottom). This is consistent with what might be expected during the deformation of a woven composite (i.e. longitudinal yarns straightening and transverse yarns bucking) and such information is invaluable for the modelling of mechanical properties.

The ability to map local yarn geometries, as shown in Figs. 6 and 7, is unique to μXRD for many systems. For example, optical methods are unable to study interlacing yarn geometries and are also restricted to translucent matrix materials. Although samples can be sectioned, this precludes in situ deformation and only gives access to isolated cross-sections [14]. As an alternative, X-ray computed microtomography (micro-CT) can resolve geometric information for many multiphase materials. However, most polymer–polymer systems have insufficient phase contrast for this technique. It is therefore usually limited to systems containing non-polymer fibres, and/or polymer matrices doped with contrast-enhancing additives [15, 16].

In-plane yarn orientation

Whilst meridional reflection intensities allow out-of-plane yarn tilt to be determined, azimuthal reflection positions reveal average fibre orientations within the detector plane. For bidirectional systems with a sufficiently high angular difference, the in-plane orientation of warp and weft yarns can be resolved independently. Although any reflection can be used to determine this parameter, equatorial reflections are preferred because of fibre symmetry. Figure 8 shows the average angle of in-plane yarn orientation, for both the transverse and longitudinal yarns within the satin weave composite. In both cases three different strain levels are shown, with all data interpolated. Prior to deformation, periodic in-plane rotations can be observed which correlate with the fabric geometry shown in Fig. 6. These correspond to yarn interlace points within the fabric where yarns are displaced by the tightly woven structure. Deformation has no impact upon these periodic displacements. However, new features appear for transverse yarns during deformation, extending from the edges of the drilled hole longitudinally along the stress axis.

The vertical 'streaks' which appear during deformation in Fig. 8 reflect localised regions of opposing in-plane orientation, which exclusively affect the transverse yarns. These originate due to the strain disparity between discontinuous and unbroken longitudinal yarns surrounding the drilled hole. This strain disparity results in shear forces which are transferred to the transverse fibres through inter-fibre friction and the resin matrix. As they cross this boundary, they exhibit a clockwise rotation on one side and an anticlockwise rotation on the other giving rise to the light and dark streaks shown in Fig. 8. An exaggerated schematic representation of this phenomenon is shown in Fig. 9. In this case lines have been used to represent the microgeometry of transverse yarns and the shearing effect which gives rise to the observed in-plane rotations. Two transverse slices are also shown, taken through zones above and below the hole. These reveal a gradual variation exists in yarn orientation between the two shear boundaries. The results shown in Figs. 8 and 9 demonstrate how the stress

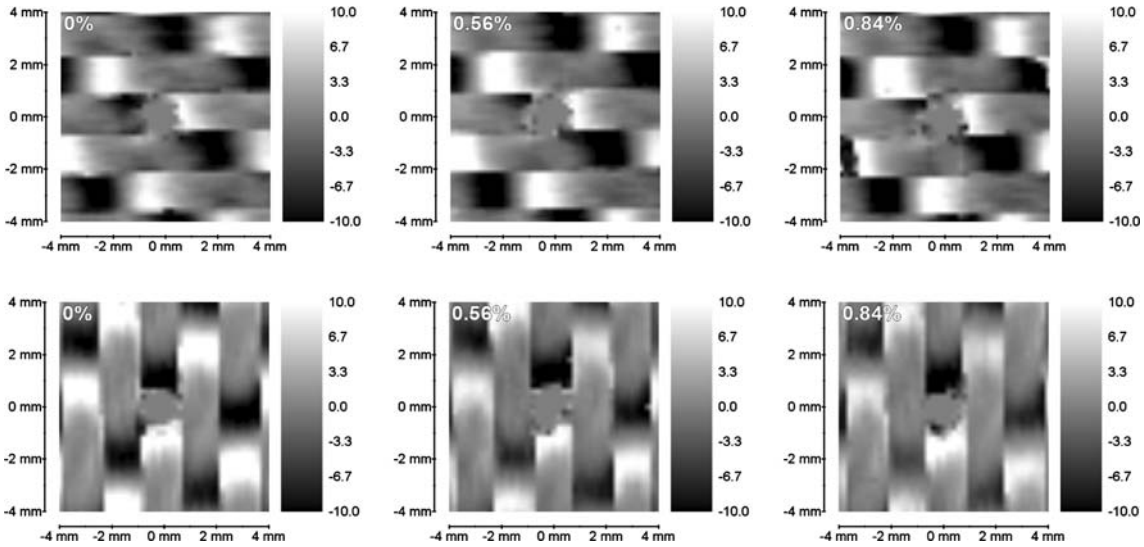

Fig. 6 Average out-of-plane fibre tilt angle (in degrees) for transverse (top) and longitudinal (bottom) yarns within the satin woven composite at three different strain levels (strain axis is vertical)

Fig. 7 The average variation of out-of-pane tilt angle (in degrees) for transverse (top) and longitudinal (bottom) yarns within linear slices across the scan area, and at three different strain levels

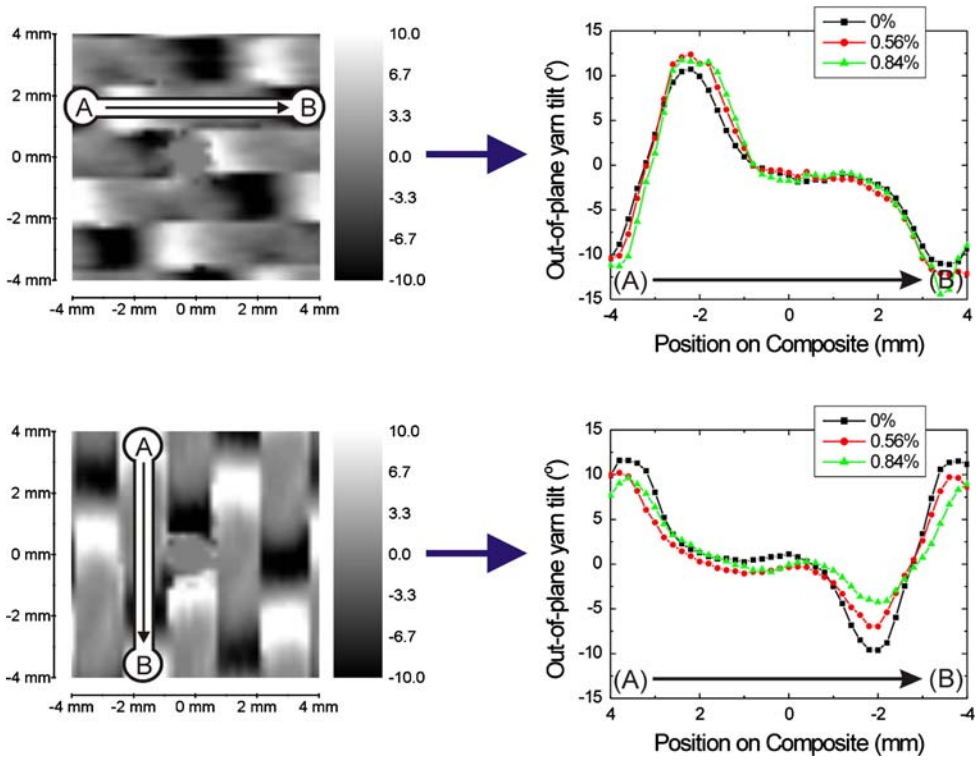

field around discontinuities such as rivet holes can influence the local geometry of the fabric.

Axial fibre stress

It has been demonstrated in Figs. 6–9 how μXRD can be used to determine the local geometry of lamina composites. However, as shown previously for model systems [2–5], diffraction data can also indicate local axial fibre stresses. This can be determined by calculating longitudinal crystal lattice distortions (crystal strain) from changes in meridional layer line position. With this information coupled with the material's crystal modulus parameter (and therefore assuming uniform stress), local axial fibre stress can be estimated. For this calculation, it is also assumed that fibres within the unloaded specimen are unstressed (i.e. negligible residual stresses exist within the system). The axial fibre stress calculation is somewhat more difficult in this

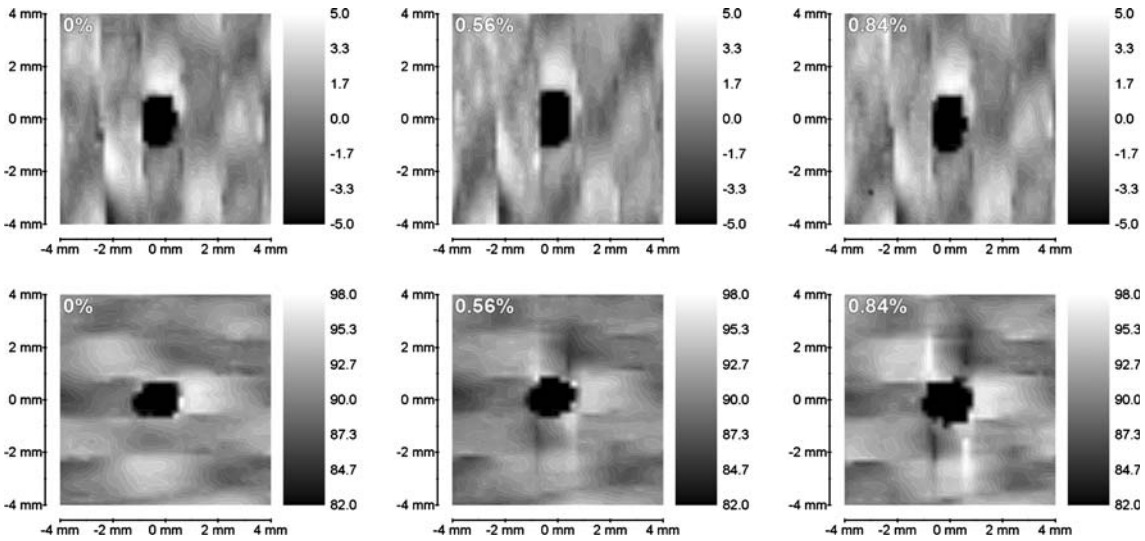

Fig. 8 Average in-plane fibre orientation (in degrees) for transverse (top) and longitudinal (bottom) yarns within the woven composite at three different strain levels (strain axis is vertical)

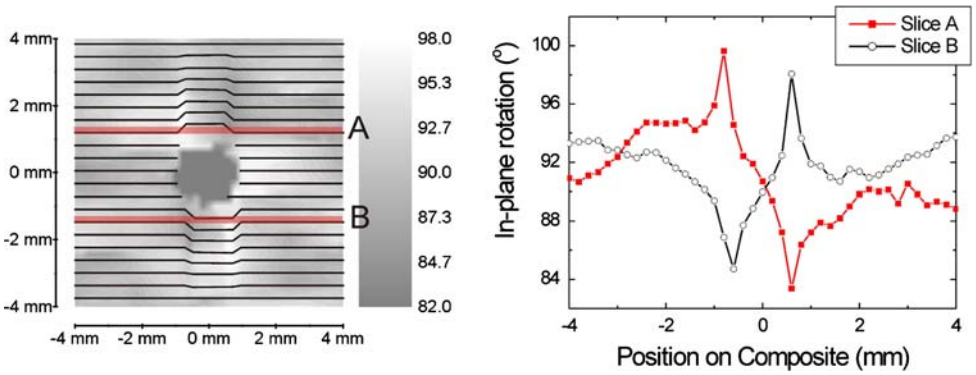

Fig. 9 (left) Exaggerated schematic demonstrating the effect of a strain disparity between discontinuous and continuous longitudinal yarns on the interlacing transverse yarns. The local shear forces give rise to highly localised in-plane rotations. (right) Variation in in-plane yarn orientation over linear slices taken above and below the hole position

geometry compared to idealised systems [2–5]. This is due to the interlacing nature of a woven sample. For modest out-of-plane angular tilts (within ± 5°), averaging reflections between hemispheres eliminates the influence of tilt on crystal lattice determination. However, beyond this range crystal strain can no longer be calculated directly. For this reason, all axial fibre stress results shown within this study are filtered to only include those within this 10° out-of-plane angular range. Beyond these values, data points have been removed (set to black) to avoid confusion. As an additional consequence of this, all stress data are also shown uninterpolated.

Figure 10 shows the spatial variation in average axial fibre stress, for both the transverse and longitudinal yarns in the woven composite at three different strain levels. It can be seen that during deformation there is a significant difference in the stresses that develop in the longitudinal and transverse yarns. The longitudinal yarns become subjected to a fluctuating axial tension that follows the geometry of the woven structure. It should be noted in that the longitudinal fibres are not subjected to axial tension above and below the hole since stress cannot be transferred along the discontinuous fibres and is instead transferred via the matrix (and inter-fibre friction) to surrounding fibres. In contrast to the longitudinal yarns, it can be seen that the transverse yarns develop an increasing axial compression when the longitudinal strain is increased as a result of the Poisson contraction in the composite.

Figure 11 shows selected slices representing the evolution in average axial fibre stress for longitudinal and transverse yarns. In both cases a 3-mm slice has been selected, which shows data within the ± 5° angular limit. This method of visualisation further highlights the development of compression in transverse yarns and tension in longitudinal yarns with macroscopic strain. It also reveals, however, that whereas local fibre stress approximately doubles in longitudinal fibres for an additional 0.32% macroscopic strain, compression of the transverse yarns does not increase proportionally. There is also a consistent difference in stress within the longitudinal fibres themselves, with axial fibre stress being slightly higher near to the ends of the slice region (Fig. 11). This probably reflects

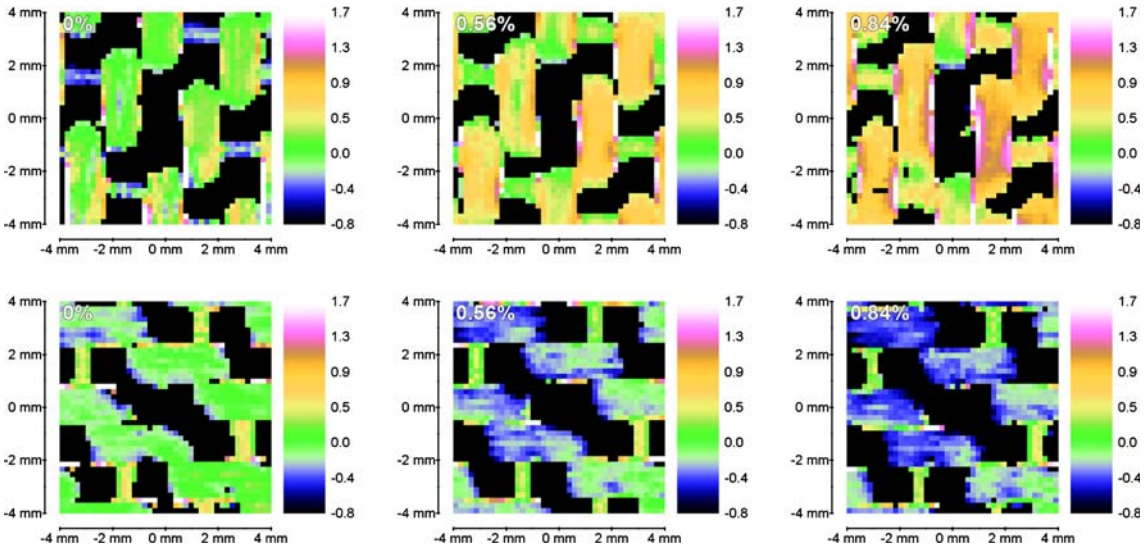

Fig. 10 Axial Fibre stress (in GPa) in the transverse (top) and longitudinal (bottom) yarns in the woven composite at three different strain levels (strain axis is vertical)

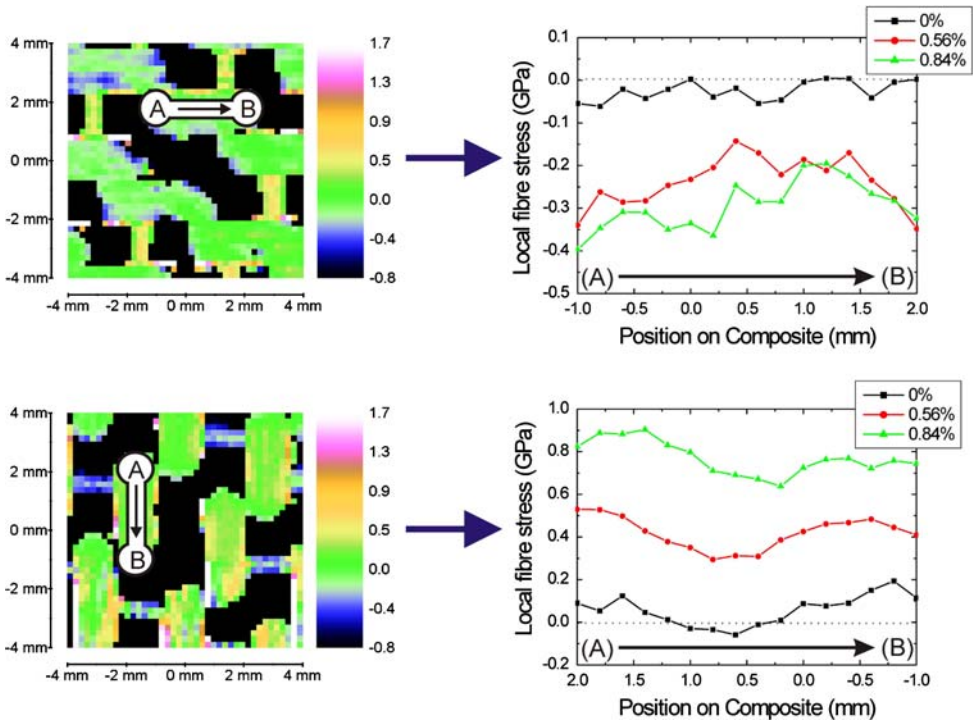

Fig. 11 Average variation of axial fibre stress for transverse (top) and longitudinal (bottom) within linear slices of 3 mm length, and at three different strain levels

an increase in tension where the fibres interlace. These points of stress concentration do not appear to decrease significantly with increasing macroscopic strain.

There are very few techniques available which can determine stresses directly within embedded fibres in a composite under load. Techniques such as electronic speckle pattern interferometry (ESPI) can only map local strains at the surface of the sample [17]. Meanwhile, although micro-Raman spectroscopy can probe local stresses in a woven composite [14], it is unable to provide any information on yarns that are underneath crossing yarns. The results shown in Figs. 10 and 11 show the potential of this approach for monitoring stresses within complex fabric geometries. Although the axial stress data presented is limited to fibres within a 10° out-of-plane angular range, this limitation could be eliminated. One possibility would be to employ suitable correction factors derived from a calibration experiment. These would then allow axial fibre stress to be corrected for of out-of-plane tilt, providing access to a much larger angular range.

Local resin thickness

Another parameter which defines the mechanical performance of a FRC is the geometry of the resin matrix. Local variations in resin thickness or zones of poor impregnation will lead to heterogeneous mechanical properties. It has previously been demonstrated that μXRD can be used to approximate the local resin volume within model composite systems [2]. This relies upon the proportionality between the isotropic scattering contribution of the resin and the volume of resin within the region illuminated by the X-ray beam [2]. A similar approach can be applied in this case to map resin volume in a woven composite sample during deformation. For this, an integration region is required which contains only the resin scattering contribution.

The local variation of resin scattering intensity is shown in Fig. 12. The position of the hole at the centre of the sample is clearly visible at all strain levels. Figure 12 shows that local resin thickness appears to fluctuate over the entire sample area. These variations persist as macroscopic strain increases and appear to be partly correlated with the woven fabric structure shown in Fig. 6. This demonstrates that in this particular sample, resin impregnation was relatively heterogeneous. Intensity maxima at yarn intersections probably correspond to excess resin lying within crevices created by the weave structure. It is worth pointing out that some point-to-point variations between strain levels are anticipated. This can be attributed to the use of a beam dimension which is much smaller than the scan resolution. Consequently, successive scans (at different strain levels) illuminate slightly different regions of the sample, giving rise to local variations between scans. Meanwhile, the high scattering intensity directly surrounding the hole itself is an artefact. At this position the fabric structure is highly disordered due to damage induced by drilling. This high intensity corresponds to a contribution from misaligned fibres whose equatorial reflections fall within the same q-range and azimuthal angle as the resin integration region.

The variation of resin scattering intensity shown in Fig. 12 demonstrates the potential of this technique for mapping composite parameters which are difficult to obtain using other methods. Such information is an important (yet often neglected) parameter for interpreting the mechanical performance of composite materials. Coupled with the geometric data from the fabric itself, this information allows virtually all aspects of the lamina composite geometry to be defined within a model.

Conclusions

The technique of μXRD is unique for studying multiphase systems such as FRCs. Its ability to show variations in reciprocal space as a function of sample position can be exploited as a novel composite imaging technique. Unlike other methods, it is not constrained to model composite systems and can therefore assess many parameters that are otherwise inaccessible. For example, micro-Raman spectroscopy is an alternative and widely used method of assessing local stresses within embedded fibres [14, 18]. However, micro-Raman is only compatible with certain polymer/matrix combinations and is more restricted in terms of sample geometry.

The real novelty of the μXRD approach lies in its ability to simultaneously resolve local stresses and details of the sample geometry. This capability has been demonstrated in this study for a woven structure during in situ deformation. From the calculation of average fibre tilt out of the detector plane, the fabric weave geometry has been resolved in detail. Meanwhile, the calculation of local in-plane yarn orientation allows shear stress concentrations to be resolved. Finally, variations in axial crystal lattice spacings indicate the distribution of axial fibre stress, which can then be related to geometrical features.

The μXRD method is also well suited for coupling with other experimental and theoretical techniques. For example, simultaneous micro-Raman spectroscopy could provide a more detailed picture of stress transfer in complex systems through its ability to probe both amorphous and crystalline fractions [19]. ESPI could allow local stresses at the surface of a composite to be compared with internal stresses. Alternatively, simultaneous small-angle X-ray scattering

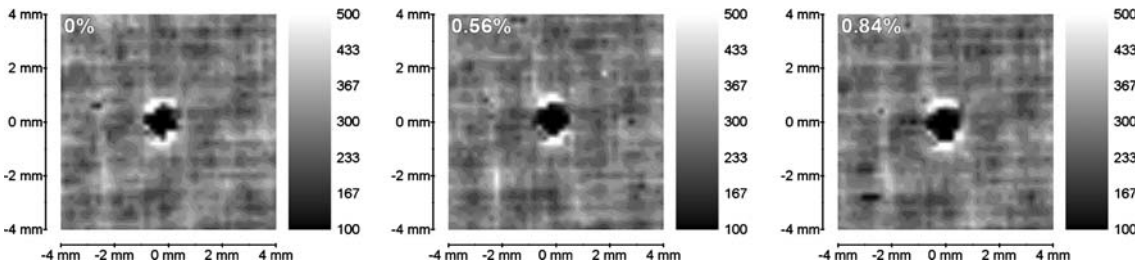

Fig. 12 Variation of resin scattering intensity as an approximation of local resin thickness (in microns) at three different strain levels

(SAXS) could be used to monitor interfacial debonding. The μXRD technique has also been employed to obtain information about the microstructure of the polymer matrix in a composite [20, 21]. The results of the present study also provide useful information for modelling [22, 23], especially as the geometry of the composite system probed experimentally could be incorporated into an FE model. Finally, it can be used as a method to assess existing analytical models [8, 24].

Acknowledgements The authors are grateful to Dr. Damien Bannister of SP Systems Ltd. for supplying the woven composite lamina and to Teijin Co Ltd. for supplying the Twaron fibres. Dr. Manfred Burghammer's technical support at the ID13 beamline was especially appreciated. This research was supported by the EPSRC (Grant code EP/C002164/1).

References

1. Riekel C, Davies RJ (2005) Curr Opin Colloid Interf Sci 9:396
2. Young RJ, Eichhorn SJ, Shyng YT, Riekel C, Davies RJ (2004) Macromolecules 37:9503
3. Eichhorn SJ, Bennett JA, Shyng YT, Young RJ, Davies RJ (2006) Compos Sci Technol 66:2197
4. Shyng YT, Bennett JA, Young RJ, Davies RJ, Eichhorn SJ (2006) J Mater Sci 41:6813. doi:10.1007/s10853-006-0211-8
5. Shyng YT, Eichhorn SJ, Young RJ, Davies RJ (2007) Compos Interf 14:351
6. Davies RJ, Riekel C, Bennett JA, Eichhorn SJ, Young RJ (2007) Appl Phys Lett 91:044102
7. Pullman D, Schaff JR (1998) Mech Compos Mater Struct 5:309
8. Hu FZ, Soutis C, Edge EC (1997) Compos Struct 37:223
9. Hammersley AP, Riekel C (1989) Synchrotron Radiat News 2:24
10. Davies RJ (2006) J Appl Crystallogr 39:262
11. Davies RJ (2006) J Appl Crystallogr 39:267
12. Shuaib AN, Al-Sulaiman FA, Hamid F (2004) Mach Sci Technol 8:449
13. Durao LMP, de Moura MFSF, Marques AT (2006) Compos Part A 37:1325
14. Lei SY, Young RJ (2001) Compos Part A 32:499
15. Lavoie JA, Adolfson E (2001) J Compos Mater 35:2077
16. Schilling PJ, Karedla BR, Tatiparthi AK, Verges MA, Herrington PD (2005) Compos Sci Technol 65:2071
17. Toubal L, Karama M, Lorrain B (2005) Compos Struct 68:31
18. Young RJ, Day RJ (1989) Brit Polym J 21:17
19. Davies RJ, Burghammer M, Riekel C (2005) Appl Phys Lett 87:264105
20. Feldman AY, Gonzalez MF, Wachtel E, Moret MP, Marom G (2004) Polymer 45:7239
21. Feldman AY, Larin B, Berestetsky N, Marom G, Weinberg A (2007) J Macromol Sci Part B-Phys 46:111
22. Potluri P, Manan A (2007) Compos Part A-Appl Sci Manuf 38:1216
23. Potluri P, Thammandra VS (2007) Compos Struct 77:405
24. Xia Z, Okabe T, Curtin WA (2002) Compos Sci Technol 62:1141